Proc. Natl. Acad. Sci. USA
Vol. 89, pp. 9429–9433, October 1992
Immunology

Three-dimensional structure of two crystal forms of FabR19.9 from a monoclonal anti-arsonate antibody

(crystal structure/hapten binding/complementarity-determining regions/combining-site rearrangement)

MARIE-BERNARD LASCOMBE*†, PEDRO M. ALZARI*, ROBERTO J. POLJAK*, AND ALFRED NISONOFF‡

*Immunologie Structurale, Unite de Recherche Associée 359 Centre National de la Recherche Scientifique, Institut Pasteur, 25 rue du Dr. Roux, 75724 Paris Cedex 15, France; and ‡Rosenstiel Research Center, Brandeis University, Waltham, MA 02254

Contributed by Alfred Nisonoff, April 28, 1992

ABSTRACT **The three-dimensional structure of FabR19.9 from a well-characterized anti-*p*-azobenzenearsonate monoclonal antibody has been determined by x-ray diffraction techniques in two crystalline forms (I and II) to a resolution of 2.8 and 2.7 Å, respectively. Essentially the same tertiary and quaternary structure of the Fab is observed in the two forms. The major difference resides in the intermolecular contacts, which are interpreted to favor an irreversible transition from the metastable form I to the more stable form II. The third complementarity-determining region of the heavy chain (H3) folds back over the combining site and requires rearrangement for hapten binding. This dynamic requirement on H3 is consistent with its mobility in the structure and can explain hapten binding to an otherwise inaccessible antibody combining site.**

The anti-*p*-azobenzenearsonate (anti-Ar) antibodies of A/J and BALB/c mice have been the subject of a wide variety of studies in different laboratories (1–6) and constitute a good model system for correlation of the three-dimensional structure of antibodies with their physiological properties. About half of the anti-Ar antibodies produced in A/J mice, after immunization with Ar conjugated to keyhole limpet hemocyanin, express an intrastrain cross-reactive idiotype designated CRI_A (1, 2). Some monoclonal anti-Ar antibodies (mAbs) derived from immunized A/J mice, including mAb R19.9 (IgG2b, κ), share some but not all idiotopes associated with CRI_A (7). The incomplete expression of CRI_A is principally due to its heavy chain (H-chain) structure; hybrid molecules containing R19.9 light chains (L chains) and H chains from a CRI_A^+ mAb strongly express CRI_A (7). The Fab fragment of mAb R19.9 has been crystallized in different forms and the structure of form I has been determined by x-ray diffraction techniques to 2.8 Å resolution (8). This crystallographic study provided a correlation between three-dimensional structure, amino acid sequences, and idiotypic markers of strain A/J anti-Ar antibodies and permitted tentative conclusions about the conformation of the hapten binding site of mAb R19.9.

In this communication, we report on the refinement of the atomic coordinates of crystals of FabR19.9 form I, on the determination of the structure of form II, and on the conclusions from a comparison of the three-dimensional structures in the two crystalline forms.§

MATERIALS AND METHODS

Form II crystals of the Fab fragment of A/J anti-Ar mAb R19.9 were obtained as described (9). The space group is monoclinic, $P2_1$, with unit cell parameters a = 42.0 Å, b = 80.6 Å, c = 75.2 Å, and β = 90.2° and one Fab molecule in the asymmetric unit. Form I crystals (9) (monoclinic space group $P2_1$, a = 43.3 Å, b = 80.8 Å, c = 75.1 Å, and β = 96.0°) were not observed in these crystallization experiments.

A diffraction data set was collected from two crystals using a Siemens-Xentronics area detector and a graphite monochromator mounted on a Rigaku RU-200 rotating anode generator. The raw data frames were reduced to structure factor amplitudes (F) using the XENGEN software package (10). A total of 41,617 measured intensities were merged to give 16,492 unique reflections to 2.5 Å resolution with an overall R merge $[\Sigma\mathbf{h}|I(\mathbf{h}) - \langle I(\mathbf{h})\rangle|/\Sigma\langle I(\mathbf{h})\rangle]$ of 8.0%. However, since only a small number of reflections had $I > 2\sigma(I)$ in the resolution shell 2.7–2.5 Å, refinement was performed using the observed reflections to 2.7 Å resolution.

A rotation function search was carried out independently for the variable ($V = V_H + V_L$) and constant ($C = C_H1 + C_L$) regions of the Fab fragment using program ROTING (11) and the reported (8) structure of R19.9 form I (Brookhaven National Laboratory Protein Data Bank code 1F19) as the search model. The largest peaks were well above background and corresponded to a 7° (V) or 4° (C) rotation around an axis approximately parallel to the crystallographic twofold axis. As these values are in good agreement with the observed difference (≈6°) in the unit cell β angle between both crystal forms, the resulting model could be directly positioned in the form II unit cell. The model was initially subjected to a constrained–restrained least-squares refinement (COREL; ref. 12) at low resolution (4.5 Å), followed by a first round of simulated annealing refinement (XPLOR; ref. 13) using all data to 2.7 Å. The R factor was 23.8% after refinement of tightly restrained atomic temperature factors.

The largest shifts from the starting model were observed for residues in the third complementarity-determining region (CDR) of the H chain (H3). Therefore, the entire H3 loop (V_H residues 99–113) was omitted from the model and rebuilt after three rounds of simulated annealing refinement alternated with manual model building using FRODO (14). Since parts of the C region and the V–C interface presented either poor density or bad stereochemistry as in the initial model (8), the whole refinement procedure was repeated using as starting model the refined structure of FabE225 (15), from an anti-idiotopic mouse mAb having the same isotype, IgG_{2b}, κ. Comparison of the results from both refinements indicates that the poor quality of the electron density map in parts of the C region is a consequence of molecular flexibility or

Abbreviations: Ar, *p*-azobenzenearsonate; CDR, complementarity-determining region; F, structure factor amplitude; F_o, observed F; F_c, calculated F; H, heavy; L, light; H2 and H3, CDR2 and CDR3 of H chain; mAb, monoclonal antibody; V_H, V_L, C_H1, and C_L, variable and constant domains of H and L chains; CRI, cross-reactive idiotype.

†To whom reprint requests should be addressed.

§The atomic coordinates and structure factors have been deposited in the Protein Data Bank, Chemistry Department, Brookhaven National Laboratory, Upton, NY 11973 (references 2F19 for the revised coordinates of form I and 1FA1 for form II).

The publication costs of this article were defrayed in part by page charge payment. This article must therefore be hereby marked "*advertisement*" in accordance with 18 U.S.C. §1734 solely to indicate this fact.

crystal disorder rather than a bias introduced during refinement. The final model converged to an *R* factor of 18.9% for 9855 observed reflections [$F > 3\sigma(F)$] in the resolution range 6–2.7 Å; the rms deviations from ideal bond lengths and angles are 0.014 Å and 3.5°, respectively.

The refined model of FabR19.9 in crystal form II was rotated back to the form I unit cell and used as a starting model for refinement against the original 2.8-Å diffractometer data set (8) since no crystals of this form could be obtained in the new crystallization trials. After three rounds of simulated annealing refinement alternated with manual model building (requiring only minor local modifications), the refinement converged to an *R* factor of 18.2% for 10,340 observed reflections [$F > 3\sigma(F)$] between 6 and 2.8 Å. The rms deviations with respect to ideal values were 0.014 Å in bond lengths and 3.4° in bond angles. Omit maps (16) for both models (forms I and II) showed continuous density for most of the main chain, with the exception of solvent-exposed loops in the C region, which show large temperature factors. Electron density corresponding to the distal part of H3 also appears discontinuous in omit maps, although $2F_o - F_c$ maps show good density (F_o, F observed; F_c, F calculated). This region, modeled (8) in an open conformation protruding into the solvent, could now be rebuilt in a close conformation, folded back into the antigen-binding site. Further refinement was attempted on models lacking residues 101–109 to detect possible multiple conformations of H3. However, the less-than-optimal quality of the electron density precludes a clear conclusion on this issue. Although electron density features of the final maps could be interpreted as water molecules, no attempt was made to include them in the model.

RESULTS AND DISCUSSION

Electron Density Map. A few residues show disallowed Φ,Ψ values for the main-chain torsion angles. These positions are mostly associated with solvent-exposed loops in regions of poorly defined density, such as C_L Asp-151 and C_H1 Gln-182 and Ala-184. The error in coordinates is between 0.25 and 0.35 Å for each model as estimated by the method of Luzzati (17).

The $(2F_o - F_c)$ electron density maps of form II crystals contoured at 1σ show a good overall agreement with the model, although as generally observed in Fab structures, the map is better for the L than for the H chain and for the V than for the C domain. The core of the subunits as well as the interfaces between H and L chains are in strong, continuous electron density. Notwithstanding the lack of intramolecular contacts, the "switch" regions connecting the C and V domains are well defined in the electron density due to crystal packing interactions. Electron density is also good for the CDR loops with the exception of Lys-55 and Tyr-57 of H2 protruding into the solvent, and residues 101–104 at the tip of H3 affected by large temperature factors.

Some loops in the vicinity of the interdomain space between the V and C subunits correspond to weak electron density, correlated with higher temperature factor values. Local discontinuities of the electron density map are observed around V_L Asp-41, V_H Gly-42, and C_H1 Gln-182. Also, the distal extremity of the C region is poorly defined, in particular the loop between C_H1 residues 168 and 174. Breaks in the continuity of the electron density map are observed for C_L residues Asp-151, Leu-181, Thr-182, Asp-184, and C_H1 residues Ser-201 and Gln-202. The H-chain loop between residues 137–148 and the L-chain C-terminal region (residues 210–214) are also poorly defined and characterized by large temperature factors.

Description of the Structure. The overall quaternary structure of the Fab molecule is as reported (8) and consistent with other known Fab molecules. It presents an elongated conformation with an elbow angle (between the pseudodyad axes relating the V and C domains of the two chains) of 178° in the two crystal forms. A similarly elongated conformation was reported for another anti-Ar, Fab36–71 (18). Interactions involving residues from the V_L and C_L subunits, which may stabilize the elongated conformation, are observed in the two anti-Ar Fabs. In Fab36–71, Glu-80 makes a hydrogen bond with Ser-168 across the V_L–C_L interface. Although position 80 is occupied by histidine in FabR19.9, the interaction (presumably involving water-mediated hydrogen bonds) is also observed.

The variations of residue-averaged temperature factors follow closely the alternating β-strands and loops along the polypeptide chain. Although both the antigen-binding site and the end of the C region are exposed to solvent and essentially not involved in crystal packing interactions, it is the loops at the end of the latter that appear more flexible with the exception of the distal end of H3, which also has large temperature factors.

Compared to the reported (8) structure of FabR19.9 form I, the general features of the current structure, such as the elbow angle and the rotation–translation operations relating the domains, are unchanged. However, additional refinement has resulted in significant deviations throughout the whole structure. C^α coordinates of individual subunits superimpose with rms deviations between 1.1 and 1.9 Å. These values result from remodeling many β-strand connecting loops. The largest deviation is for H3, with displacements of main-chain atoms as large as 5–6 Å, since this loop has been remodeled in a "closed" conformation, folding back over the antigen combining site. The other CDRs are not significantly affected by the present refinement; rms deviations between single CDRs from the previous and current models are in the range 0.5–1 Å. The framework region between V_L residues 5 and 15 has also been modified and five loops, C_L 185–189, 200–204 and C_H1 135–145, 168–172, and 196–204, show average deviations of main-chain atoms >3 Å. However, these loops have large temperature factors.

Comparisons of Crystal Forms I and II. The refined models of forms I and II indicate that the structures are very similar. Local differences are directly correlated with either poorly defined density or large temperature factors. The tips of H2 and H3 protrude out from a relatively flat antigen-binding surface and show the largest deviations between the models of the two crystal forms. Other significant differences are concentrated in β-strand connecting loops, many of which (at or around C_L positions 150, 157, and 187 and C_H1 position 196) appear to be a consequence of different crystal packing interactions.

Superposition of all main-chain atoms from the entire molecule results in an rms deviation of 0.6 Å, comparable to the values obtained when the individual subunits are superimposed (0.5 Å for V_L, 0.6 Å for V_H and C_L, and 0.7 Å for C_H1). This indicates that the Fab behaves as a rigid unit in the two different packing environments, conserving the elbow angle as well as the spatial relationship between the domains.

Crystal Packing Interactions. The behavior of crystals, which either spontaneously or upon x-ray irradiation undergo the transition form I → form II (but not the reverse), and the fact that both forms grow under the same crystallization conditions suggest that form I represents a thermodynamically metastable state. The pattern of accessible surface occluded by intermolecular contacts is comparable in the two crystal forms, giving no clue to explain the energetic preference for one of the forms. However, an analysis of residue-averaged intermolecular interactions [using the energy potential parameters provided with XPLOR (13) and the refined coordinates of both models] strongly suggests a strengthening of interactions in two particular contact regions of form II. In one of these regions, a salt bridge occurs between V_H Lys-19

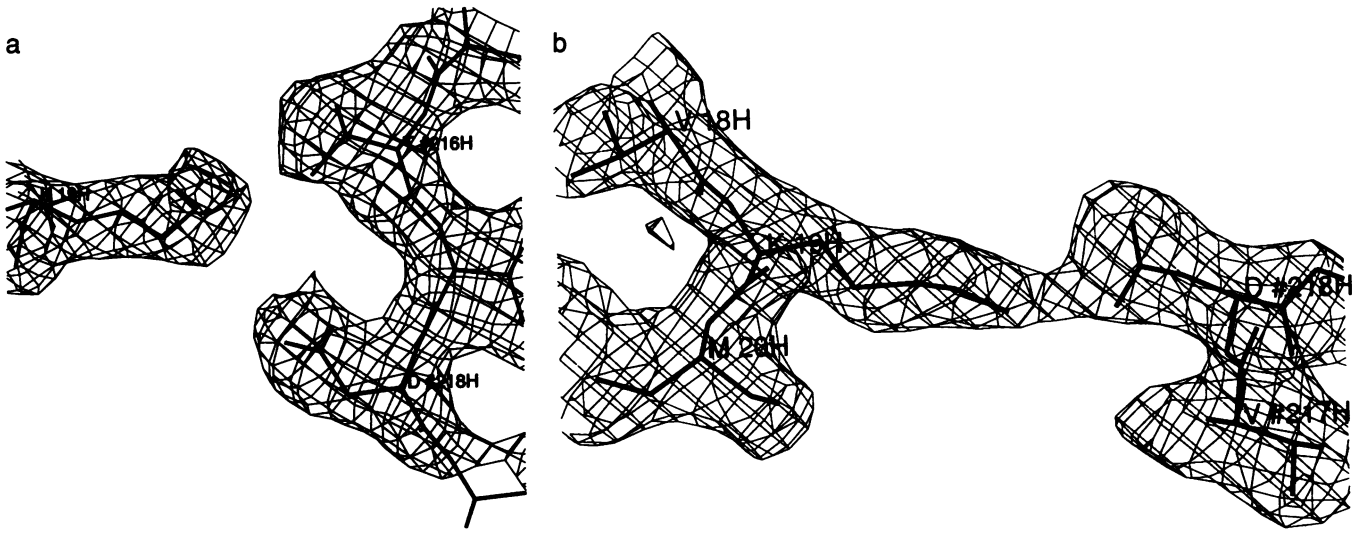

FIG. 1. Intermolecular interaction between V_H Lys-19 and V_H Asp-218 from a neighboring molecule in crystal forms I (*a*) and II (*b*). In the latter, a salt bridge is clearly indicated by the electron density map.

and C_H1 Asp-218 from a neighboring molecule in form II crystals. The electron density for the side chains is clearly defined in the two structures (Fig. 1), although it is less clear why the bridge is not observed in form I crystals, as both residues belong to rather flexible polypeptide loops. The observed differences are unlikely to arise from constraints imposed during refinement since partial charges of ionizable side chains had been set to zero throughout the simulated annealing calculations. The second region, which shows a significant rearrangement of interactions, involves the largely exposed C_L loop 150–154, which is in contact with residues from three different loops of a neighboring molecule: L chain His-80, Asp-167, Ser-168, Lys-169 and C_H1 Ser-171. Although His-80 in form II crystals is relatively distant to make direct contact with C_L Glu-154, a water-mediated interaction is suggested by the electron density map. Note that these contacts do not include residues such as asparagine or glutamine, which could undergo deamination as a result of protein purification and storage and could thus lead to different intermolecular interactions and different crystal forms.

In the rest of the structure, essentially the same pattern of intermolecular contacts is seen in both crystal forms, an observation confirmed by both accessible surface and energy calculations. This analysis suggests that enthalpic strengthening of localized contacts contributes to the thermodynamic preference of crystal form II. Although this is a plausible explanation, it has to be borne in mind that the limited resolution precludes modeling of protein-bound solvent molecules, which may also contribute significantly to the stability of crystal packing.

Conformation of the CDRs. The CDR loops of R19.9 form I have similar conformations to those described (8), with the exception of the entirely rebuilt H3. Well-defined electron density is observed for most of the CDR main-chain and side-chain atoms in both crystal forms. As mentioned above, only the H2 side chains of Lys-55 and Tyr-57 and the distal residues 102–106 of H3 are in weak electron density in the final $2F_o - F_c$ maps, consistent with the fact that these two loops protrude away from a relatively flat recognition surface.

No significant differences in conformations are observed for the CDRs between the two current models (Fig. 2). The rms deviations between individual loops range between 0.4 and 0.7 Å. Moreover, their conformations predicted as proposed by Chothia *et al.* (19, 20) show a remarkable agreement with the observed conformations (Fig. 2). For the entire V region, the rms deviations of C^α positions between predicted and observed individual loops are of the order 1.4–1.8 Å. These values reduce to 0.5–1.0 Å when CDRs are optimally matched on an individual basis, suggesting that, at least for FabR19.9, the conformations of the CDRs depend on their amino acid sequences and not on tertiary structure interactions.

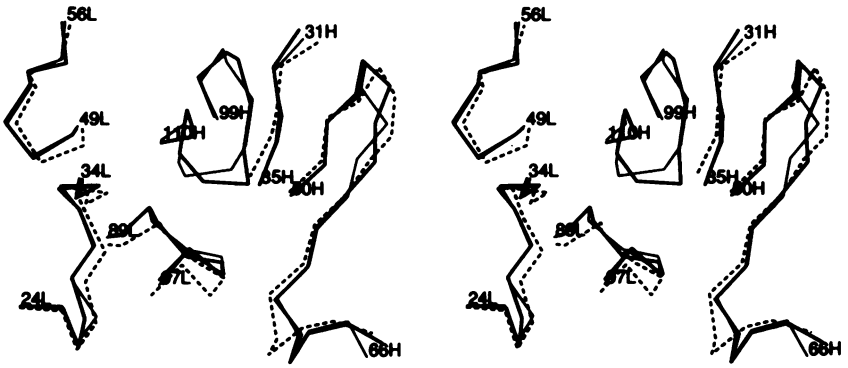

FIG. 2. CDRs of R19.9 (C^α backbone). Form I (thick line) and form II (thin line) have been superimposed. The predicted conformation of the CDR loops (C. Chothia and A. Lesk, personal communication) is indicated by the dotted line; H3 conformation was not predicted. L1, residues 24L–34L; L2, residues 49L–56L; L3, residues 89L–97L; H1, residues 31H–35H; H2, residues 50H–56H; H3, residues 99H–110H.

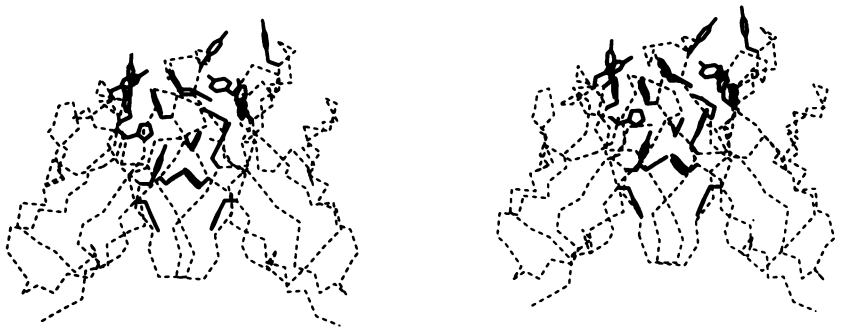

FIG. 3. Stereoview of the distribution of aromatic residues in the V region of R19.9. C^{α} backbones of V_H (*Right*) and V_L (*Left*) subunits are indicated by dashed lines.

Comparison with the amino acid sequences of murine mAbs R16.7 (21) and 36–65 (22), bearing the major idiotype of the anti-Ar response, shows that R19.9 has a four-residue insertion at H3 near the junction of genetic segments D and J_H2 (D, diversity; J, joining), as well as a one-amino acid deletion at position 101. This change in the length of H3 could explain why R19.9 does not fully express the major CRI of anti-Ar antibodies of the A/J strain (7, 23). Indeed, H3 folds back into the combining site toward L3 (Fig. 2), thus hindering accessibility to the central region of the antigen-binding site as well as affecting expression of the major idiotype.

Interactions between aromatic residues are particularly remarkable in R19.9, with an unusually large concentration of aromatic residues in the neighborhood of the active site and in the interface V_H–V_L (Fig. 3). Some of these aromatic side chains, such as V_L Tyr-50 and V_H Tyr-32, Tyr-57, and Tyr-101, protrude into the solvent exposing most of their side-chain accessible surface. The rings of V_L Tyr-49 and V_H Tyr-110 and, to a lesser extent, V_H Phe-100 are involved in stacking interactions. In crystal form I, the hydrophobic part of V_L Arg-96 side chain is stacked between V_H Tyr-109 and Trp-47 (Fig. 4; see below). Another interaction that could be described as partial stacking involves residues V_H Tyr-101, Tyr-32, and Tyr-27 at the molecular surface. The V_H–V_L interface mainly involves the following aromatic residues: V_L, Tyr-32, Tyr-36, Tyr-49, Tyr-50, Phe-97, and Phe-98; V_H, Trp-47, Phe-95, Tyr-109, Tyr-110, Phe-111, and Trp-114. Some of these aromatic residues may also be involved in direct interactions with the hapten (see below).

Hapten-Binding Site. Attempts at crystallizing FabR19.9 complexed to Ar haptens such as *m*-azobenzene-*p*-arsonic-3-(*p*-hydroxyphenyl)propionic acid or *p*-aminobenzenearsonic acid were unsuccessful (9). After diffusion of equimolar amounts of the hapten into Fab crystals, these became yellow, indicating binding, and subsequently dissolved irrespective of variations introduced in the composition of storing buffers to stabilize the crystals. These results led to the proposal that either the haptens were bound to the combining site hindering intermolecular contacts necessary for a stable crystalline structure or that hapten binding causes conformational changes that may affect intermolecular contacts. The latter postulate was favored since *p*-aminobenzenearsonic acid is a small hapten that could be bound without interfering with intermolecular side-chain contacts. In their study of Fab36–71, Strong *et al.* (18, 24) experienced similar difficulties in obtaining crystalline Fab–hapten complexes. However, they were able to model the bound hapten from a low-resolution image of an Ar-containing heavy atom derivative. In their model of the complex, polar interactions with the Ar moiety of the hapten could be provided by the side chains of V_L Arg-96, V_H Trp-47, Asn-35, Ser-99 and a protein-bound water molecule, whereas toward the molecular surface the phenyl group of the hapten might be stacked between the aromatic rings of V_H residues Tyr-106 and Tyr-50 (numbering as in figure 8 of ref. 24).

All residues proposed by Strong *et al.* (18, 24) to interact with hapten are highly conserved in >80 anti-Ar antibodies that have been sequenced. The same residues are found at these positions in R19.9 and, also, the putative binding site is very similar to that of Fab36–71 (Fig. 4). However, the greater length of R19.9 H3 relative to that of 36–71 creates important differences between the two structures. In R19.9, V_H Tyr-109 points inward and fills up the cavity occupied by Ar in the hapten–Fab36–71 model (24).

During refinement of the two crystal forms of FabR19.9, two alternative conformations for the side chains of V_L Arg-96 and V_H Tyr-109 were observed (Fig. 4). The conformation in form II is similar to that observed in Fab36–71, stabilized by hydrogen bonds between one terminal nitrogen from V_L Arg-96 and the main-chain carbonyl oxygens of Gly-91 and Ala-93 (18, 25). In FabR19.9, additional hydrogen-bond interactions are made by the other terminal nitrogen of V_L Arg-96 and the carbonyl oxygen of H3 Asp-105. In the alternative conformation observed in form I, the hydrophobic

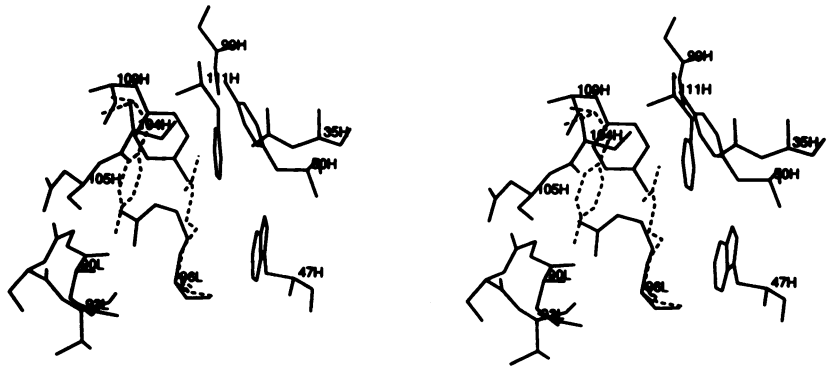

FIG. 4. Stereoview of the putative hapten-binding site for R19.9 crystal form II. The alternative conformation adopted by the side chains of residues V_H Arg-96 and V_H Tyr-109 in crystal form I is shown by dashed lines.

moiety of Arg-96 is stacked between V_H Tyr-109 and V_H Trp-47. Additional stability is provided by a hydrogen bond between the OH group of V_H Tyr-109 and the main-chain carbonyl oxygen of V_L Thr-93 (distance, 3.1 Å). Although no attempts were made to refine either observed conformation by using partial occupancies, we may assume that in solution the combining site will flip back and forth between them. This suggests either that Ar binding to FabR19.9 is different than in Fab36–71 or, more probably, that some rearrangement of the R19.9 binding site is required, since neither the conformation of form I or form II would allow for binding of the Ar hapten. Creation of a cavity in FabR19.9 to bind Ar requires a conformational change of the H3 loop allowing the side chain of V_H Tyr-109 to rotate back into the solvent and, at the same time, opening the entrance to the binding site for an external ligand. This "dynamic" requirement, consistent with the high temperature factors of H3, could explain why binding of an Ar hapten dissolves the Fab crystal. Small but significant side-chain and main-chain rearrangements have been observed in other antibody–ligand complexes (16, 26–28).

The hapten-binding affinity of mAb R19.9 is related to the energetics of the folding of H3 that permits binding of benezenearsonate derivatives; an energy requirement would be expected to lower the binding affinity. The K_a value for the interaction of R19.9 with the hapten (*p*-azobenzenearsonic acid)-*N*-acetyl-L-tyrosine is $5.2 \times 10^5\ M^{-1}$ (29). This value is comparable to those of many other CRI_A-related mAbs from spleen cells taken during a secondary response (29) and exceeds that of the germ-line-encoded CRI_A^+ mAb 36–65 by a factor of 2 (30). This suggests that the free energy required to expose the hapten-binding site is not large. It may be noted that the four-amino acid insertion in the H3 loop of R19.9 (as compared to the germ-line-encoded CRI_A^+ H chain) can readily account for the fact that R19.9 does not express all of the idiotopes associated with CRI_A.

We thank Ginette Boulot for help and advice with the crystallization experiments. This work was supported by grants from the CNRS, Pasteur Institute, and by Grant AI-24272 from the U.S. National Institutes of Health.

1. Kuettner, M. G., Wang, A. L. & Nisonoff, A. (1972) *J. Exp. Med.* **135**, 579–595.
2. Greene, M. I., Nelles, M. J., Sy, M.-S. & Nisonoff, A. (1982) *Adv. Immunol.* **32**, 253–300.
3. Rathbun, G., Sanz, I., Meek, K., Tucker, P. & Capra, J. D. (1988) *Adv. Immunol.* **42**, 95–164.
4. Manser, T., Wysocki, L. J., Margolies, M. N. & Gefter, M. L. (1987) *Immunol. Rev.* **96**, 141–162.
5. Brown, A. R., Lamoyi, E. & Nisonoff, A. (1981) *J. Immunol.* **126**, 1264–1268.
6. Meek, K., Jeske, D., Slaoui, M., Leo, O., Urbain, J. & Capra, J. D. (1984) *J. Exp. Med.* **160**, 1070–1086.
7. Gill-Pazaris, L. A., Lamoyi, E., Brown, A. R. & Nisonoff, A. (1981) *J. Immunol.* **126**, 75–79.
8. Lascombe, M.-B., Alzari, P. M., Boulot, G., Saludjian, P., Tougard, P., Berek, C., Haba, S., Rosen, E. M., Nisonoff, A. & Poljak, R. J. (1989) *Proc. Natl. Acad. Sci. USA* **86**, 607–611.
9. Mariuzza, R. A., Amit, A. G., Boulot, G., Saludjian, P., Saul, F. A., Tougard, P., Poljak, R. J., Conger, J., Lamoyi, E. & Nisonoff, A. (1984) *J. Biol. Chem.* **259**, 5954–5958.
10. Howard, A. J., Gilliland, G. L., Finzel, B. C., Poulos, T. L., Ohlendorf, D. H. & Salemne, F. R. (1987) *J. Appl. Crystallogr.* **20**, 383–387.
11. Navaza, J. (1987) *Acta Crystallogr.* **A43**, 645–653.
12. Sussman, J. L., Holbrook, S. R., Church, G. M. & Kim, S. H. (1977) *Acta Crystallogr.* **A33**, 800–804.
13. Brünger, A. T., Kuriyan, J. & Karplus, M. (1987) *Science* **235**, 458–460.
14. Jones, T. A. (1984) *J. Appl. Crystallogr.* **17**, 244–248.
15. Bentley, G. A., Boulot, G., Riottot, M.-M. & Poljak, R. J. (1990) *Nature (London)* **348**, 254–257.
16. Bhat, T. N. & Cohen, G. H. (1984) *J. Appl. Crystallogr.* **17**, 244–248.
17. Luzzati, V. (1952) *Acta Crystallogr.* **5**, 802–810.
18. Strong, R. K., Campbell, R., Rose, D. R., Petsko, G. A., Sharon, J. & Margolies, M. N. (1991) *Biochemistry* **30**, 3739–3748.
19. Chothia, C. & Lesk, A. M. (1987) *J. Mol. Biol.* **196**, 901–917.
20. Chothia, C., Lesk, A. M., Tramontano, A., Levitt, M., Smith-Gill, S. J., Air, G., Sheriff, S., Padlan, E. A., Davies, D., Tulip, W. R., Colman, P. M., Spinelli, S., Alzari, P. M. & Poljak, R. J. (1989) *Nature (London)* **342**, 877–883.
21. Siegelman, M. & Capra, J. D. (1981) *Proc. Natl. Acad. Sci. USA* **78**, 7679–7683.
22. Siekevitz, M., Gefter, M. L., Brodeur, P., Riblet, R. & Marshak-Rothstein, A. (1982) *Eur. J. Immunol.* **12**, 1023–1032.
23. Lamoyi, E., Estess, P., Capra, J. D. & Nisonoff, A. (1980) *J. Exp. Med.* **152**, 703–711.
24. Strong, R. K., Petsko, G. A., Sharon, J. & Margolies, M. N. (1991) *Biochemistry* **30**, 3749–3757.
25. Rose, D. R., Strong, R. K., Margolies, M. N., Gefter, M. L. & Petsko, G. A. (1990) *Proc. Natl. Acad. Sci. USA* **87**, 338–342.
26. Edmundson, A. B., Ely, K. R. & Herron, J. N. (1984) *Mol. Immunol.* **21**, 561–576.
27. Stanfield, R. L., Fieser, T. M., Lerner, R. A. & Wilson, I. A. (1990) *Science* **248**, 712–719.
28. Rini, J. M., Schulze-Gahmen, U. & Wilson, I. A. (1992) *Science* **255**, 959–965.
29. Kresina, T. F., Rosen, S. M. & Nisonoff, A. (1982) *Mol. Immunol.* **19**, 1433–1439.
30. Rothstein, T. L. & Gefter, M. L. (1983) *Mol. Immunol.* **20**, 161–168.